ARMY RESEARCH LABORATORY

Shadow Zone Boundary Limitation of the Effective Acoustical Turbulence Scattering Volume Using the Turbule Ensemble Model

Harry J. Auvermann and George H. Goedecke

ARL-TR-2234

September 2000

Army Research Laboratory

Adelphi, MD 20783-1197

ARL-TR-2234 **September 2000**

Shadow Zone Boundary Limitation of the Effective Acoustical Turbulence Scattering Volume Using the Turbule Ensemble Model

Harry J. Auvermann

Computational and Information Sciences Directorate, ARL

George H. Goedecke

Department of Physics, New Mexico State University

Abstract

The Turbule Ensemble Model (TEM) was developed to handle acoustical scattering from anisotropic inhomogeneous turbulence. A turbule is a localized atmospheric inhomogeneity. TEM, then, represents a turbulent region by a collection of turbules of different sizes. Since acoustic sources and sensors are omnidirectional, the scattering volume of the TEM region is ill defined. Scattering properties of individual turbules in TEM show that the majority of scattering originates from a constricted volume, called the effective scattering volume. This is true for a region of homogeneous turbulence and is anticipated to be true for a region of inhomogeneous turbulence, although no calculations have been made. Estimates have been given of the size and shape of the effective scattering volume as a function of turbule size for an experiment conducted in homogeneous turbulence and a uniform atmosphere. In this report, homogeneous turbulence is retained, but an upwardly refracting atmosphere is assumed, resulting in a shadow zone. Inclusion of the shadow zone boundary further limits turbule sizes and locations from which significant signals reach the detector. The finding is that large turbules are less effective scatterers and that effective scattering volumes are large enough for the number of small turbules to be large. Implications of this finding are discussed.

Contents

Figures

Tables

1. Introduction

Six papers were presented at the Battlefield Atmospherics Conferences and other conferences that deal with acoustic scattering by atmospheric turbulence. The sixth paper (Auvermann and Goedecke, 1995a) contains a summary of the first five papers; this report is an extension of that paper and the fifth paper in the series (Auvermann et al, 1994). Here we refer to the fifth paper in that series (Auvermann et al, 1994) as paper A and the sixth paper (Auvermann and Goedecke, 1995a) as paper B. Experimental evidence shows that atmospheric turbulence near the ground is neither homogeneous nor isotropic, two conditions required for the usual statistical model of turbulence to be valid. An alternate model, termed the Turbule Ensemble Model (TEM), consists of a collection of turbules of different sizes. A turbule is an isolated inhomogeneity of either temperature or velocity. In TEM, the scattering pattern of individual turbules is assumed known. The analysis proceeds by the assumption of a distribution function for the sizes, and then location of the turbules of each size, randomly, within the atmospheric region of interest. The shadow zone signal is then the summation of the contributions from each turbule.

Acoustical signals of interest to the Army are, in general, low frequency. The importance of this is that wavelengths are large compared to the dimensions of either source or detector. Therefore, both source and detector are nearly omnidirectional and thus cannot serve to define a scattering volume. Paper A (Auvermann et al, 1994) addressed the problem of determining the volume from which significant scattering can occur (called the effective scattering volume (ESV)) for an elementary spherical shell volume. Paper B (Auvermann and Goedecke, 1995a) addresses the determination of ESV for a homogeneous turbulence region isolated from the ground. In this report, a shadow zone boundary (SZB) is introduced into the scenario, with the remaining properties of the medium assumed to be homogeneous. The full power of TEM for addressing scattering from anisotropic inhomogeneous turbulence has not been exploited as yet. The signal from anisotropic inhomogeneous turbulence may be calculated by populating the ESV with randomly oriented and located turbules and summing the scattered power. Presently, the summation process is carried out with the use of integrals over mathematically defined distributions. A distinction must be made between isotropic turbulence and isotropic scattering. Isotropic turbulence, in the context of TEM, refers to an ensemble of turbules that has uniformly distributed orientation vectors. Such an ensemble has anisotropic scattering properties that delimit ESV as a function of turbule size. Only velocity turbulence will be considered in this report.

2. Background

In this section, the results obtained in papers A and B are recounted. Paper A was the first step in the process of using the scattering properties of turbules to define ESV. The calculation there was simply of the total scattering cross section of the turbules in a spherical shell surrounding the detector. The source was assumed to be a long distance away, so that the incident signal was a plane wave. The turbulence had parameters appropriate for a 10-m height above the ground. However, in the simplified calculation, the source and detector were assumed to be far enough above ground as to be in a free atmosphere. Sound speed gradients were assumed to be zero, so that no shadow zones were present. The largest turbule considered had a 10-m radius, which was appropriate for the 10-m height of the scenario. The frequency and wavelength were 500 Hz and 0.688 m, respectively. The scattering pattern of the large turbules was found to greatly limit the region of space from which the scattered signal could reach the detector. In spite of this small region of space, the scattering properties of these large turbules dominated the scattering cross section. This scenario (a plane wave from the source in a medium of infinite size) cannot be extended to calculate the signal from an infinite space, because the scattered signal at the detector would be infinite. Although the signal from more distant spherical shells falls off as $1/r^2$, the total volume of the shell increases by r^2, leaving the signal from each shell the same. When the total is computed for an increasing distance r, the total increases without bound.

In paper B, the distant source scenario was abandoned in favor of an experimental scenario, with the source and detector finitely separated. The $1/r^2$ loss from source to scatterer, coupled with the $1/r^2$ loss from scatterer to detector, served to produce a finite signal at the detector. ESV was found to vary from 4.4 m^3 for the largest turbule to 2311 m^3 for a turbule of 0.44 m radius. Figure 1 (taken from paper B) shows the intersection locus of the scattering volume limit with the vertical plane containing the source and detector for three different turbule sizes.

Figure 2 depicts the scenario of this report. The coordinates are x, y, and z, with the origin on the ground beneath the source. The source and detector heights are h_S and h_D, respectively. The wind flows from the direction of the detector toward the source. The simplest wind speed profile will be used to produce a shadow zone, namely, a uniform gradient model. The plan—the execution of which is discussed in section 5—is to introduce a wind-driven shadow zone boundary into the scenario of figure 2 and then calculate the ESV in a manner similar to the calculation in paper B. A reasonable wind speed gradient will show an appreciably sized shadow zone over the experiment distance chosen (320 m). Two matters not addressed in paper B must be dealt with first: (1) calculating parameters (turbule spacing and

Figure 1. Scattering volume shape with no shadow zone.

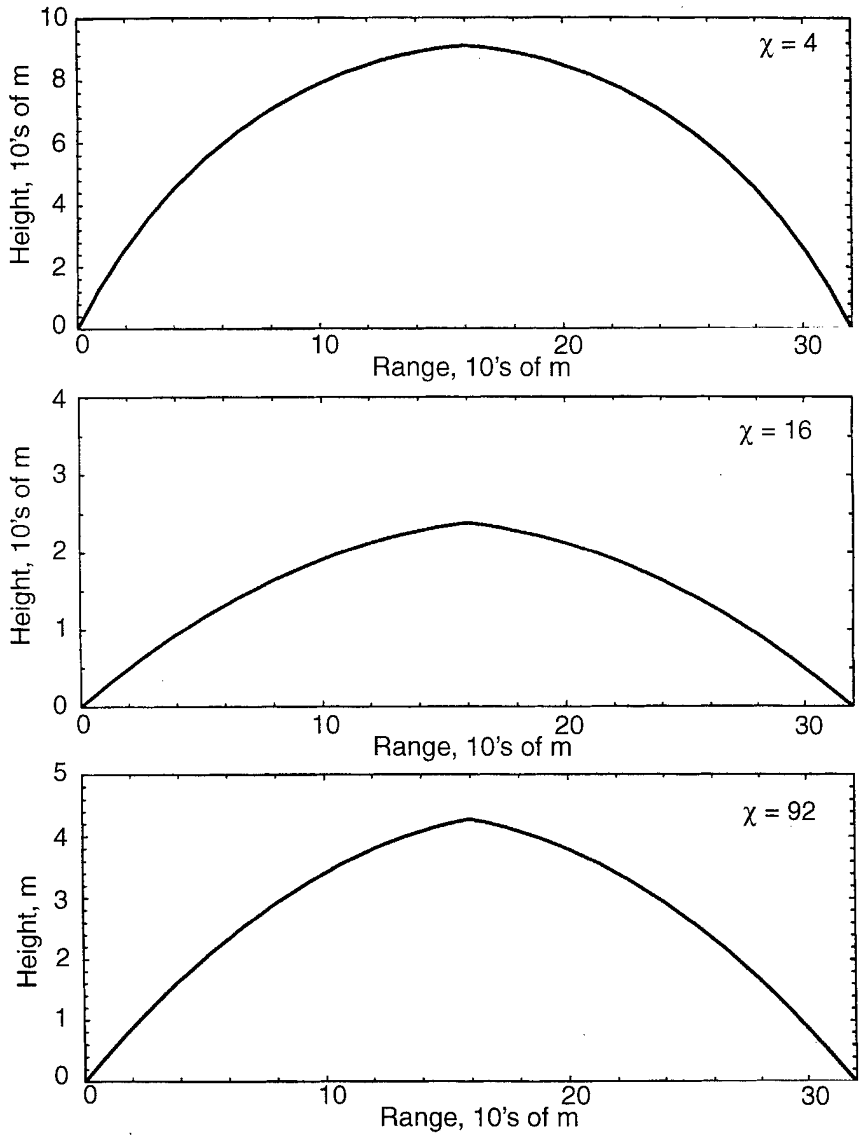

Figure 2. Calculation geometry.

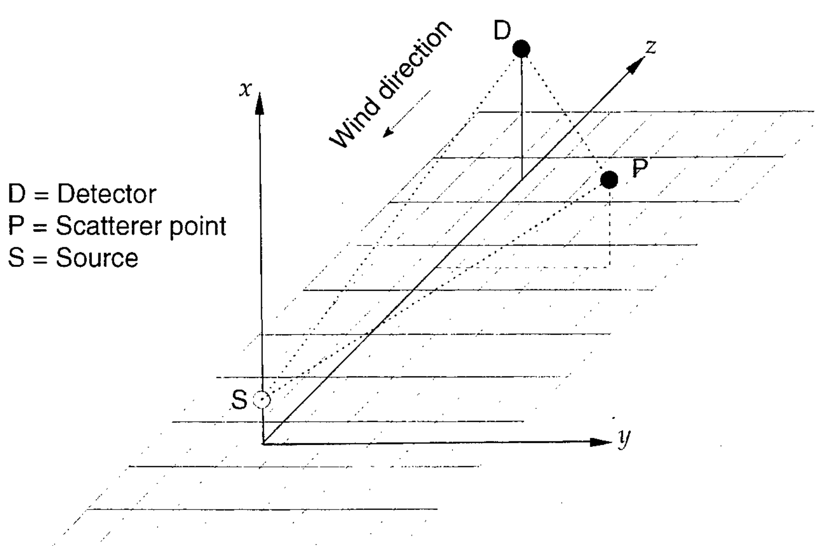

size increment) for a representative turbulence distribution and (2) developing an equation for the SZB surface. These matters are discussed in the next two sections.

Symbols for some of the variables and parameters used in this report are summarized in the following list:

a = turbule characteristic size (m)

c = sound speed, 3.44 $m{\cdot}s^{-1}$

E_D^v = total irradiance at detector

e_D^v = relative irradiance at the detector

f = acoustic wave frequency = 500 Hz

θ = spherical coordinate system polar angle

ϕ = spherical coordinate system azimuthal angle

k = $2\pi/\lambda$

l = ratio of turbule average spacing to turbule characteristic size a

μ = turbule size ratio increment parameter

λ = wavelength, m = 0.688 m

N_1 = total number of turbules of the largest size

r = spherical coordinate system radial distance

R_S = source irradiance reference distance = 1.0 m

R_{SD} = source detector distance = 320 m

R_{SP} = source (point P) distance

R_{PD} = (point P) detector distance

$\sigma_v(\psi, \chi)$ = velocity turbule total scattering cross section

v_{a0} = turbule flow velocity parameter

$v_a(r, \theta)$ = turbule velocity function

V_s = scattering volume

χ = size parameter = ka

X_u = upper limit of size parameter considered = 91.325367

X_m = maximum in the size parameter integration

X_n = minimum in the size parameter integration

ψ = scattering angle

Ω = magnitude of the angular velocity vector

3. Turbule Spacing and Size Increment Parameters

The turbule spacing and size increment parameters are the l and μ, respectively, from the list of parameters in section 2. The size increment parameter will be determined by energy conservation considerations for a turbule velocity distribution of (Goedecke, 1992)

$$\begin{aligned} \vec{v}(\vec{r}) &= \Omega\, \hat{z} \times \vec{r} \exp\left(-r^2/a^2\right) , \\ v_a(r, \theta) &= (v_{a0}/a)\, r \sin(\theta) \exp\left(-r^2/a^2\right) , \end{aligned} \tag{1}$$

where the rotation axis has been set along the z-axis. Because of rotational symmetry, the latter expression shows the dependence on the spherical coordinates of r and θ. The total kinetic energy of the turbule $T(a)$ will be the integral of one-half the density ρ times the square of this velocity:

$$T(a) = \left(\frac{\rho\, v_{a0}^2}{2\, a^2}\right) \int_0^\infty dr\, r^4 \exp\left(-2\, r^2/a^2\right) \int_0^\pi d\theta\, [\sin(\theta)]^3 \int_0^{2\pi} d\phi = \left(\frac{\pi\, \rho\, \Gamma\,(5/2, 0, \infty)}{3 \times 2^{1/2}}\right) v_{a0}^2\, a^3 , \tag{2}$$

where Γ is the Generalized Incomplete Gamma Function (Wolfram, 1991). The ratio of the energy of the largest turbule to that of the next smaller one using the former velocity relation (Auvermann, 1994) is the following:

$$\frac{T(a_1)}{T(a_2)} = \left(\frac{v_1^2\, a_1^3}{v_2^2\, a_2^3}\right) = \left(\frac{a_1}{a_2}\right)^{11/3} = [\exp(\mu)]^{11/3} = 2; \quad \mu = (3/11) \ln(2) = 0.1890 . \tag{3}$$

The first expression in equation (3) results if the largest turbules break up into two turbules of the next lower size and split energy equally. There are 49 size classes in this distribution, from the largest at 10 m (denoted by the subscript 1) to the smallest at 1.146 mm (denoted by the subscript 49).

Next, recall the expression for the velocity structure constant (Goedecke et al, 1998), which is

$$\begin{aligned} C_v^2 &= \left(\frac{0.69}{\mu}\right) \left(\frac{N_1\, a_1^3}{V_s}\right) \left(\frac{v_1}{a_1^{1/3}}\right)^2 J_{14/3}^v(0, \infty) , \\ J_{14/3}^v(0, \infty) &= \int_0^\infty dy\, y^{14/3} \exp\left(-y^2/2\right) = 2^{11/6}\, \Gamma\,(17/6, 0, \infty) = 6.1455 . \end{aligned} \tag{4}$$

For fractal scaling, each turbule size class has the same l (Goedecke et al, 1998). N_1/V_s is the concentration of the largest turbules, so that the second bracket is l^{-3}. The value of v_1 that we have been using is 3.44 $\mathrm{m \cdot s^{-1}}$. To obtain a value for the structure parameter, we resort to the literature (Brown and Clifford, 1976). The velocity structure constant expression is given as

$$C_v^2 = 0.04 + 0.33\, z^{-2/3} , \tag{5}$$

where z is the height in meters. Substitution of 10 for z gives a value for the velocity structure parameter of 0.1111 $m^{4/3} \cdot s^{-2}$. Rewriting equation (4) gives the value of l:

$$l = \left(\frac{0.69\, v_1^2\, J_{14/3}^{v}(0, \infty)}{C_v^2\, \mu\, a_1^{2/3}} \right)^{1/3} = \left(\frac{(0.69)\,(3.44)^2\,(6.1455)}{(0.1111)\,(0.1890)\,(10)^{2/3}} \right)^{1/3} = 8.0148\ . \qquad (6)$$

If the centers of vortices are closer than 2.8 times the diameter of an individual vortex, the mutual distortion can be expected to cause the vortices to disintegrate (Moore and Saffman, 1975, eq (13), p 468). This number of 2.8 would translate into a value of 5.6 if the spacing were compared to the vortex radius. Thus, the value of 8 from equation (6) is reasonable, although the exact relation of the vortex diameter from Moore and Saffman's work to the turbule characteristic size (a) of the model is not known.

4. Derivation of Shadow Zone Boundary Equation

For a wind speed of 3.44 m·s^{-1} at a height of 10 m and zero at the ground, the gradient $g(0)$ is 0.344 s^{-1}. A uniform gradient profile declining with increasing x produces a circular ray path (Pierce, 1989, p 385), whose radius is the length for the sound speed to extrapolate to zero or 1000 m. Negligibly small transverse curvature of ray paths is assumed, so that a ray launched in a vertical plane making an angle β with the x-z plane will remain in that plane. The sound-speed gradient is related to the component of the wind velocity in the launch plane or $g(\beta) = g(0)\cos(\beta)$. The SZB is the limit ray circle that contains the source point and is tangent to the ground. For $\beta = 0$, the equation of this circle is given in the following:

$$\begin{aligned} &(x_S - r_{c0})^2 + (z - z_{c0})^2 = r_{c0}^2\,; \qquad r_{c0} = c/g(0)\,; \qquad z_{c0} = \left(2\, r_{c0}\, h_S - h_S^2\right)^{1/2} \,. \\ &\quad x_S = \left\{ r_{c0} - \left[r_{c0}^2 - (z - z_{c0})^2 \right]^{1/2} \right\} \,. \end{aligned} \tag{7}$$

The last form in equation (7) is the useful one, since the height of the SZB at a variable z will later determine a limit for an integral. For the circle in a plane at an angle β with the x-z plane, in equation (7), replace $g(0)$ with $g(\beta)$ and (z, z_{c0}) by analogous distances, say, $(\rho_\beta, \rho_{c\beta})$. Then, replace $\cos(\beta)$ and $(\rho_\beta, \rho_{c\beta})$ with the appropriate functions of the variable coordinates (y, z):

$$\begin{aligned} &(x_S - r_{c\beta})^2 + (\rho_\beta - \rho_{c\beta})^2 = r_{c\beta}^2\,; \qquad \rho_\beta = (y^2 + z^2)^{1/2}\,; \qquad \cos(\beta) = z/\rho_\beta \,. \\ &\quad r_{c\beta} = c/(g(0)\cos(\beta))\,; \qquad \rho_{c\beta} = \left(2\, r_{c\beta}\, h_S - h_S^2\right)^{1/2} \,. \\ &\quad x_S = \left\{ r_{c\beta} - \left[r_{c\beta}^2 - (\rho_\beta - \rho_{c\beta})^2 \right]^{1/2} \right\}, \qquad z > 0 \,. \\ &\quad\;\; = 0, \qquad\qquad\qquad\qquad\qquad\qquad z \le 0 \,. \end{aligned} \tag{8}$$

The last expression for x_S, where z is less than or equal to 0, recognizes that propagation in the negative direction (down wind) will not experience a shadow zone. This is unimportant, except for algorithm purposes. There is also an SZB associated with the detector. Signal scattered from turbules below the detector SZB will not reach the detector. This boundary will be of the same form, except that the z coordinate will turn to $-z_D$, and then the z_D will be replaced by $(R_{SD} - z)$

$$\begin{aligned} &(x_D - r_{c\alpha})^2 + (\rho_\alpha - \rho_{c\alpha})^2 = r_{c\alpha}^2\,; \qquad \rho_\alpha = \left[y^2 + (R_{SD} - z)^2\right]^{1/2}\,; \qquad \cos(\alpha) = (R_{SD} - z)/\rho_\alpha \,. \\ &\quad r_{c\alpha} = c/(g(0)\cos(\alpha))\,; \qquad \rho_{c\alpha} = \left(2\, r_{c\alpha}\, h_D - h_D^2\right)^{1/2} \,. \\ &\quad x_D = \left\{ r_{c\alpha} - \left[r_{c\alpha}^2 - (\rho_\alpha - \rho_{c\alpha})^2 \right]^{1/2} \right\}, \qquad 0 < z < R_{SD} \\ &\quad\;\; = 0, \qquad\qquad\qquad\qquad\qquad\qquad z \ge R_{SD} \,. \end{aligned} \tag{9}$$

The integral limit mentioned above will be determined for a y-z plane point (y, z) by choice of the larger of x_S or x_D. The larger of x_S or x_D is referred to as

SZB hereafter. Figure 3 is a three-dimensional plot of equations (8) and (9), showing the SZB surfaces. Figure 4 shows the ESV surface from paper B for a size parameter of 4.0 superimposed on these SZBs.

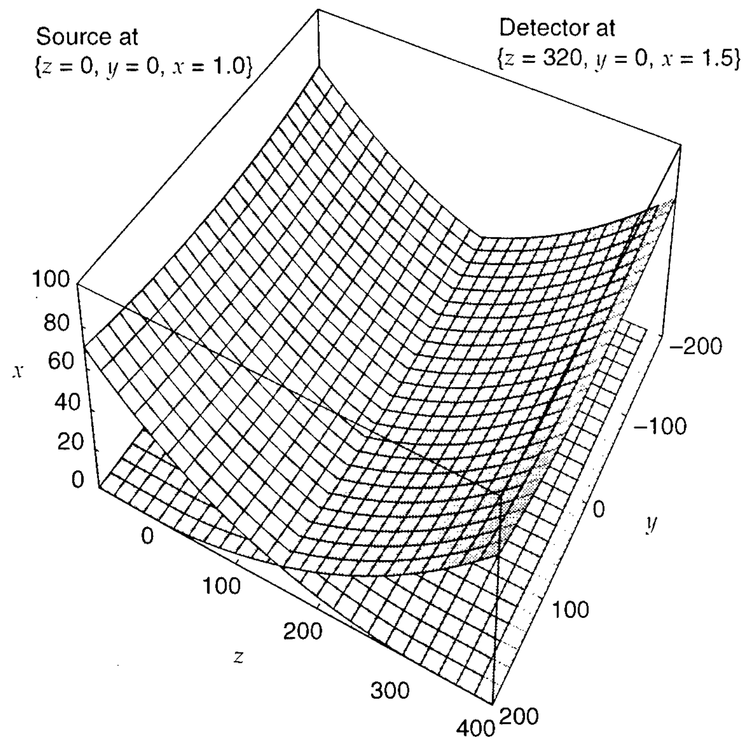

Figure 3. Shadow zone boundary surfaces.

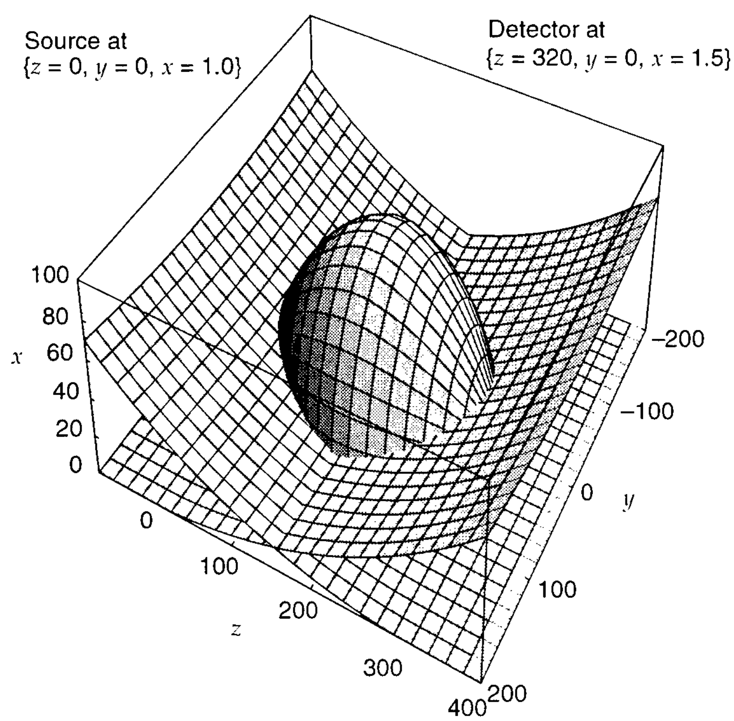

Figure 4. Effective scattering volume surface for size parameter of 4.0 superimposed on shadow zone boundaries.

5. Scattered Signal at Detector Equation

Since we make the assumption that the only influence of the wind gradient and the presence of the ground is to produce the SZB of section 4, the equation for the scattered signal at the detector will be set up in terms of the distances and angles relative to the source-detector line of figure 2. And since we also assume homogeneous, isotropic turbulence, the scattering will have rotational symmetry with respect to this line. Imposition of the SZB will produce only a rotational angle in the ϕ integration. For the velocity distribution of equation (22), the orientation averaged cross section is (Goedecke, 1992), with c_∞ as the asymptotic sound speed,

$$\sigma_v(\psi, \chi) = \left(\frac{\pi}{3}\right)\left(\frac{\Omega\, a\, \chi^4}{4\, k\, c_\infty}\right)^2 [\sin(\psi)\cos(\psi)]^2 \exp\{-\chi^2[1-\cos(\psi)]\} \ . \quad (10)$$

The total signal will be the differential signal multiplied by a differential volume with a space integration. Including integration over size parameter, the final expression is in equation (8) (Auvermann et al, 1994). The differential volume is a partial ring around the source-detector line,

$$E_D^v = \left(\frac{N_1\, E_S\, (k\, a_1)^{1/3}\, e^\mu}{24\,(e^\mu - 1)}\right)\left(\frac{\pi\, v_1\, a_1\, R_S}{c_\infty}\right)^2 \int_{Z_n}^{Z_m} dz \int_0^{Y_m} dy\, [2\, r_r\, \phi \cos(\gamma)]\, (R_{SP}\, R_{PD})^{-2}$$
$$[\sin(\psi)\cos(\psi)]^2 \int_{X_n}^{X_m} d\chi\, \chi^{14/3} \exp\{-\chi^2\,[1-\cos(\psi)]\} \ , \quad (11)$$

with the ring ending on the SZB on each side. By symmetry of the SZB with respect to the x-z plane, the differential volume is $2\, r_r(y, z)\, \phi(y, z)\, dz\, dy$, where r_r is the radius of the ring and ϕ is the ring angle between the x-z plane and the SZB intersection point. In equation (11), $(r_r, \phi, R_{SP}, R_{PD}, \psi)$ are all functions of (y, z) through the SZB height h_Z. The $\cos(\gamma)$ accounts for the inclination of the source-detector line $[\tan(\gamma) = (h_D - h_S)/R_{SD}]$. E_S is the reference irradiance.

6. Imposition of Significance Criteria

Expressions for the relative signals of interest are

$$I(Z_n, Z_m, Y_m, X_n, X_m) = \int_{X_n}^{X_m} d\chi \int_{Z_n}^{Z_m} dz \int_{0}^{Y_m} dy [2\, r_r\, \phi](R_{SP}\, R_{PD})^{-2}$$
$$[\sin(\psi)\cos(\psi)]^2\, \chi^{14/3} \exp\{-\chi^2 [1-\cos(\psi)]\}\ , \tag{12a}$$

$$I(-\infty, \infty, \infty, 0, X_n) = \int_{\infty}^{\infty} dz \int_{0}^{\infty} dy\, [2\, r_r\, \phi](R_{SP}\, R_{PD})^{-2}$$
$$[\sin(\psi)\cos(\psi)]^2 \int_{0}^{X_n} d\chi\, \chi^{14/3} \exp\{-\chi^2 [1-\cos(\psi)]\}\ , \tag{12b}$$

$$e_D^{\bar{v}} = \left(\frac{I(Z_n, Z_m, Y_m, X_n, X_m)}{I(-\infty, \infty, \infty, 0, X_n)}\right) = \Sigma\ . \tag{12c}$$

$(Z_n, Z_m, Y_m, X_n, X_m)$ are the integration limits for two conditions. The first condition is that for all space for which these limits are infinity, zero, or X_n. The objective of this report is to find limits subject to the condition that the signal is a large fraction of the infinite limit signal, equation (12b). Thus the expressions may dispense with the constant in front of the integrals in equation (11). The relative signal $e_D^{\bar{v}}$ is defined in terms of the integrals, and the significance criterion Σ is set equal to it. The meaning is that the limits are to be found that make $e_D^{\bar{v}}$ at least as great as Σ, which is thought of as being a number such as 0.99.

7. Determination of ESV

The procedure to be used is the following. The reference integral (eq 12(b)) will be calculated for the parameters specified in this report. Then, lower and upper limits for the χ integration (X_n, X_m) will be determined such that the integral will differ in each case by no more that 0.002 from the reference integral, with all other limits the same. Then the y integral will be evaluated as a function of (χ, z) to determine a table of $Y_m(\chi, z)$ values such that this integral differs no more than 0.002 from its value when the upper limit is infinity. A function that approximates this table will be determined. Finally, the integral with these limits will be calculated to show that the relative signal is greater than the criterion Σ. These criteria are summarized in table 1. Table 2 summarizes the calculated results. Table 3 has been constructed for five of the sizes of equation (3). From table 2, it is seen that the consequence of this rather simple criteria scheme was that Y_m approximated a cylinder, and the total Σ was too large. This implies that a more sophisticated scheme in which the χ dependence of the z limits is required to improve the accuracy of the results. The SZB is likely to be more like that of figure 4 than a cylinder. However, important conclusions can be drawn using the results of table 3. The SZB length l_S has been estimated from other data, and the concentration C_χ has been calculated for an l (eq (6)) of 8. Associated with the table are some numbers calculated for the second entry. This entry is the maximum contributor to the total signal. Dividing l_S by N_χ for this size gives an average spacing, as shown. Dividing the average

Table 1. Selection of significance criteria.

Goal:	Σ	= 0.99
	$\Sigma\,(X_n)$	= 0.998
	$\Sigma\,(X_m)$	= 0.998
	$\Sigma\,(Z_n)$	= 0.998
	$\Sigma\,(Z_m)$	= 0.998
	$\Sigma\,(Y_m)$	= 0.998

Table 2. Scattering volume results.

$I\,(-\infty, \infty, \infty, 0, X_u)$	= 0.456394
$I\,(Z_n, Z_m, Y_m, X_n, X_m)$	= 0.452400
Σ	= 0.9912
X_n	= 1.3249
X_m	= 52.4223
Z_n	= 44.5736 m
Z_m	= 272.8049 m
Y_m	= 816.4478 $(\chi)^{-1.31}$

Table 3. Scattering volume constituents.

χ	a_χ	r_s	l_s	V_s	C_χ	N_χ
51.80	5.67	4.63	40.00	1.350×10^3	1.072×10^{-5}	1.440×10^{-2}
16.67	1.83	20.47	120.00	7.898×10^4	3.187×10^{-4}	2.517×10^1
7.83	0.86	55.12	182.78	8.723×10^5	3.071×10^{-3}	2.678×10^3
2.52	0.28	243.51	220.49	2.054×10^7	8.897×10^{-2}	1.827×10^6
1.43	0.16	511.84	228.23	9.392×10^7	4.768×10^{-1}	4.478×10^7

χ = size parameter
a_χ = turbule radius, m
r_s = scattering volume radius, m
l_s = scattering volume length, m
V_s = scattering volume, m^3
C_χ = turbule concentration, m^{-3}
N_χ = number of turbules

Dominant scatterer has
size parameter = 16.67
Spacing in ESV = 4.767 m
Wind speed = 3.44 $m \cdot s^{-1}$
Period = 1.4 s
Experimental period = 4 s

spacing by the wind speed gives an estimate of the period that might be expected as turbules of this size are tracked through the ESV. This period of 1.4 s is close to the period from experimental results.* This fact is important because it suggests that a more accurate calculation is warranted. However, a more accurate calculation will need a realistic estimate of the size parameter division point between that part of the signal that can be obtained by integration (a continuum calculation) and those parts that must be addressed as discrete.

*Shadow zone data reported by Havelock, Stenson, and Daigle (1992) were examined privately by the authors to arrive at this estimate.

8. Conclusions

The ultimate utility of the work on ESV may be that it will afford a physical explanation of the shadow zone scattered signal fluctuations. The data from table 3 of section 7 lead to the belief that we can conclude that this variability is caused by the motion of a limited number of moderately sized turbules through the ESV. The next step in the investigation will require a more sophisticated method for determining the (z, y) limits of the scattering volume. Of equal, or even greater, importance will be the determination of the minimum population of the scattering volume as a function of size parameter that will result in insignificant fluctuations. This minimum population will determine the turbule size, which divides the sizes that must be summed over from the sizes that can be integrated.

References

Auvermann, H. J., G. H. Goedecke, and M. D. DeAntonio (1994), "The influence of scattering volume on acoustic scattering by atmospheric turbulence," *Proc. 1994 Battlefield Atmospherics Conf.*, 29 November–1 December 1994, White Sands Missile Range, NM.

Auvermann, H. J., and G. H. Goedecke (1995a), "Calculation of scattering volume limits for acoustical scattering from homogeneous turbulence using the turbule ensemble model," *Proc. Sixth Annual Ground Target Modeling and Validation Conf.*, 22–24 August 1995, Houghton, MI.

Auvermann, H. J., and G. H. Goedecke (1995b), "Shadow zone boundary limitation of the effective acoustical turbulence scattering volume using the turbule ensemble model," presented at 1995 Battlefield Atmospheric Conference, 5–7 December 1995, White Sands Missile Range, NM.

Brown, E. H., and S. F. Clifford (1976), "On the attenuation of sound by turbulence," *J. Acoust. Soc. Am.* **60** (4), pp 788–794, October 1976.

Goedecke, G. H. (1992), *Scattering of Acoustical Waves by a Spinning Atmospheric Turbule*, U.S. Army Atmospheric Sciences Laboratory, CR-92-0001-2, White Sands Missile Range, NM.

Goedecke, G. H., M. DeAntonio, and H. J. Auvermann (1998), *Structure Function Spectra and Acoustic Scattering Due to Homogeneous Isotropic Atmospheric Turbule Ensembles*, U.S. Army Research Laboratory, ARL-TR-1518, August 1998.

Havelock, D. I., M. R. Stenson, and G. A. Daigle (1992), "Phase and amplitude fluctuations in a refractive shadow," *J. Acoust. Soc. Am.* **92** (4), part 2, p 2405, October 1992.

Moore, D. W., and P. G. Saffman (1975), "The density of organized vortices in a turbulent mixing layer," *J. Fluid Mechanics* **69**, part 3, pp 465–473.

Pierce, A. D. (1989), "Acoustics," *Acoust. Soc. Am.*, Woodbury, NY.

Wolfram, S. (1991), *MATHEMATICA: A System for Doing Mathematics by Computer*, Addison-Wesley, Redwood City, CA, p 572.

Distribution

Admnstr
Defns Techl Info Ctr
Attn DTIC-OCP
8725 John J Kingman Rd Ste 0944
FT Belvoir VA 22060-6218

DARPA
Attn S Welby
3701 N Fairfax Dr
Arlington VA 22203-1714

Mil Asst for Env Sci Ofc of the Undersec of Defns for Rsrch & Engrg R&AT E LS
Pentagon Rm 3D129
Washington DC 20301-3080

Ofc of the Secy of Defns
Attn ODDRE (R&AT)
The Pentagon
Washington DC 20301-3080

Ofc of the Secy of Defns
Attn OUSD(A&T)/ODDR&E(R) R J Trew
3080 Defense Pentagon
Washington DC 20301-7100

AMCOM MRDEC
Attn AMSMI-RD W C McCorkle
Redstone Arsenal AL 35898-5240

ARL Chemical Biology Nuc Effects Div
Attn AMSRL-SL-CO
Aberdeen Proving Ground MD 21005-5423

Dir for MANPRINT
Ofc of the Deputy Chief of Staff for Prsnnl
Attn J Hiller
The Pentagon Rm 2C733
Washington DC 20301-0300

Natl Security Agency
Attn W21 Longbothum
9800 Savage Rd
FT George G Meade MD 20755-6000

Redstone Scientific Info Ctr
Attn AMSMI-RD-CS-R
Bldg 4484
Redstone Arsenal AL 35898

SMC/CZA
2435 Vela Way Ste 1613
El Segundo CA 90245-5500

TECOM
Attn AMSTE-CL
Aberdeen Proving Ground MD 21005-5057

US Army ARDEC
Attn AMSTA-AR-TD M Fisette
Bldg 1
Picatinny Arsenal NJ 07806-5000

US Army CECOM RDEC
Night Vsn & Elect Sensors Dirctrt
Attn AMSEL-RD-NV-OD F Milton
10221 Burbeck Rd Ste 430
FT Belvoir VA 22060-5806

US Army CRREL
Attn CRREL-GP R Detsch
72 Lyme Rd
Hanover NH 03755-1290

US Army Dugway Proving Ground
Attn STEDP 3
Attn STEDP-MT-DA-L-3
Attn STEDP-MT-M Bowers
Dugway UT 84022-5000

US Army Info Sys Engrg Cmnd
Attn AMSEL-IE-TD F Jenia
FT Huachuca AZ 85613-5300

US Army Missile Cmnd
Attn AMSMI-RD-AS-SS R Alongi
Redstone Arsenal AL 35898-5253

US Army Natick RDEC Acting Techl Dir
Attn SBCN-T P Brandler
Natick MA 01760-5002

Distribution (cont'd)

US Army OEC
Attn CSTE-AEC-FSE
4501 Ford Ave Park Center IV
Alexandria VA 22302-1458

US Army Simulation, Train, & Instrmntn Cmnd
Attn AMSTI-CG M Macedonia
Attn J Stahl
12350 Research Parkway
Orlando FL 32826-3726

US Army Soldier & Biol Chem Cmnd
Dir of Rsrch & Techlgy Dirctrt
Attn SMCCR-RS I G Resnick
Aberdeen Proving Ground MD 21010-5423

US Army Tank-Automtv Cmnd Rsrch, Dev, & Engrg Ctr
Attn AMSTA-TR J Chapin
Warren MI 48397-5000

US Army TRADOC Anlys Cmnd—WSMR
Attn ATRC-WSS-R
White Sands Missile Range NM 88002

US Army Train & Doctrine Cmnd
Battle Lab Integration & Techl Dirctrt
Attn ATCD-B
FT Monroe VA 23651-5850

US Military Academy
Mathematical Sci Ctr of Excellence
Attn MADN-MATH MAJ M Huber
Thayer Hall
West Point NY 10996-1786

Nav Air War Cen Wpn Div
Attn CMD 420000D C0245 A Shlanta
1 Admin Cir
China Lake CA 93555-6001

Nav Surface Warfare Ctr
Attn Code B07 J Pennella
17320 Dahlgren Rd Bldg 1470 Rm 1101
Dahlgren VA 22448-5100

Naval Surface Weapons Ctr
Attn Code G63
Dahlgren VA 22448-5000

AF Rsrch Lab
Phillips Lab Atmospheric Sci Div
Geophysics Dirctrt
Hanscom AFB MA 01731-5000

Phillips Lab Atmospheric Sci Div
Geophysics Dirctrt
Attn PL-LYP Chisholm
Kirtland AFB NM 87118-6008

NASA Marshal Spc Flt Ctr
Atmos Sci Div
Attn Code ED 41 1
Huntsville AL 35812

Armstrong Atlantic State University
Attn R C Wood
11935 Abercorn Street
Savannah GA 31419-1997

New Mexico State Univ
Dept of Physics
Attn G Goedecke
Las Cruces NM 88003-8001

Univ of Mississippi
NCPA
Attn H E Bass
University MS 38577

Dept of Commerce Ctr
Mountain Administration
Attn Spprt Ctr Library R51
325 S Broadway
Boulder CO 80303

Hicks & Associates Inc
Attn G Singley III
1710 Goodrich Dr Ste 1300
McLean VA 22102

Distribution (cont'd)

Natl Ctr for Atmospheric Research
Attn NCAR Library Serials
PO Box 3000
Boulder CO 80307-3000

NCSU
Attn J Davis
PO Box 8208
Raleigh NC 27650-8208

Director
US Army Rsrch Ofc
Attn AMSRL-RO-D JCI Chang
Attn AMSRL-RO-EN W D Bach
PO Box 12211
Research Triangle Park NC 27709

US Army Rsrch Lab
Attn AMSRL-DD J M Miller
Attn AMSRL-CI-AI-R Mail & Records Mgmt
Attn AMSRL-CI-AP Techl Pub (3 copies)
Attn AMSRL-CI-LL Techl Lib (3 copies)
Attn AMSRL-D D R Smith
Attn AMSRL-IS-EE D K Wilson
Attn AMSRL-IS-EE
H J Auvermann (5 copies)
Attn AMSRL-SE-EE Z G Sztankay
Attn AMSRL-SE-SA N Srour
Adelphi MD 20783-1197

REPORT DOCUMENTATION PAGE

Form Approved OMB No. 0704-0188

1. AGENCY USE ONLY *(Leave blank)*	2. REPORT DATE	3. REPORT TYPE AND DATES COVERED
	September 2000	FY94 to FY95

4. TITLE AND SUBTITLE Shadow Zone Boundary Limitation of the Effective Acoustical Turbulence Scattering Volume Using the Turbule Ensemble Model

5. FUNDING NUMBERS
DA PR: B53A
PE: 61102A

6. AUTHOR(S) Harry J. Auvermann (ARL), George H. Goedecke (Department of Physics, New Mexico State University)

7. PERFORMING ORGANIZATION NAME(S) AND ADDRESS(ES)
U.S. Army Research Laboratory
Attn: AMSRL-CI-EP email: auvermann@arl.army.mil
2800 Powder Mill Road
Adelphi, MD 20783-1197

8. PERFORMING ORGANIZATION REPORT NUMBER
ARL-TR-2234

9. SPONSORING/MONITORING AGENCY NAME(S) AND ADDRESS(ES)
U.S. Army Research Laboratory
2800 Powder Mill Road
Adelphi, MD 20783-1197

10. SPONSORING/MONITORING AGENCY REPORT NUMBER

11. SUPPLEMENTARY NOTES
ARL PR: 0FEJ60
AMS code: 61110253A11

12a. DISTRIBUTION/AVAILABILITY STATEMENT Approved for public release; distribution unlimited.

12b. DISTRIBUTION CODE

13. ABSTRACT *(Maximum 200 words)*
The Turbule Ensemble Model (TEM) was developed to handle acoustical scattering from anisotropic inhomogeneous turbulence. A turbule is a localized atmospheric inhomogeneity. TEM, then, represents a turbulent region by a collection of turbules of different sizes. Since acoustic sources and sensors are omnidirectional, the scattering volume of the TEM region is ill defined. Scattering properties of individual turbules in TEM show that the majority of scattering originates from a constricted volume, called the effective scattering volume. This is true for a region of homogeneous turbulence and is anticipated to be true for a region of inhomogeneous turbulence, although no calculations have been made. Estimates have been given of the size and shape of the effective scattering volume as a function of turbule size for an experiment conducted in homogeneous turbulence and a uniform atmosphere. In this report, homogeneous turbulence is retained, but an upwardly refracting atmosphere is assumed, resulting in a shadow zone. Inclusion of the shadow zone boundary further limits turbule sizes and locations from which significant signals reach the detector. The finding is that large turbules are less effective scatterers and that effective scattering volumes are large enough for the number of small turbules to be large. Implications of this finding are discussed.

14. SUBJECT TERMS Turbulence, scattering volume, acoustic shadow zone

15. NUMBER OF PAGES 23

16. PRICE CODE

17. SECURITY CLASSIFICATION OF REPORT	18. SECURITY CLASSIFICATION OF THIS PAGE	19. SECURITY CLASSIFICATION OF ABSTRACT	20. LIMITATION OF ABSTRACT
Unclassified	Unclassified	Unclassified	UL

NSN 7540-01-280-5500

Standard Form 298 (Rev. 2-89)
Prescribed by ANSI Std. Z39-18
298-102